Accuracy of gates in a quantum computer based on vibrational eigenstates

Dmitri Babikov
Chemistry Department, Marquette University, Wehr Chemistry Building, Milwaukee, Wisconsin 53201-1881

A model is developed to study the properties of a quantum computer that uses vibrational eigenstates of molecules to implement the quantum information bits and shaped laser pulses to apply the quantum logic gates. Particular emphasis of this study is on understanding how the different factors, such as properties of the molecule and of the pulse, can be used to affect the accuracy of quantum gates in such a system. Optimal control theory and numerical time-propagation of vibrational wave packets are employed to obtain the shaped pulses for the gates NOT and Hadamard transform. The effects of the anharmonicity parameter of the molecule, the target time of the pulse and of the penalty function are investigated. Influence of all these parameters on the accuracy of qubit transformations is observed and explained. It is shown that when all these parameters are carefully chosen the accuracy of quantum gates reaches 99.9%. © *2004 American Institute of Physics.* [DOI: 10.1063/1.1791635]

I. INTRODUCTION

Feynman[1] introduced the concept of a quantum computer over 20 years ago. Since that time, sophisticated quantum logic and error correction algorithms have been developed and are ongoing topics of intense research.[2] For many computational problems, the computational advantages of quantum computing are astronomical when compared to the familiar classical computer. Quantum computers are famous for their ability to crack cryptographic codes, efficiently search large databases, and easily simulate quantum systems. Each of these problems scales exponentially with the size of the system using a standard classical computer. The superposition principle in quantum mechanics effectively allows a quantum computer to process exponentially large problems using exponentially many paths through time.[2] This extreme "parallelization" of computational work in a quantum computer reduces the exponential scaling laws associated with classical computing to linear scaling laws. The realization of a quantum computer would revolutionize the computational sciences:[2] "Quantum computing would be to ordinary computing what nuclear energy is to fire."

Two primary obstacles are associated with realizing a quantum computer: (a) Identifying a physical system to represent quantum bits, and (b) implementing quantum logic operations on these quantum bits. The first demonstration of rudimentary quantum algorithms was performed using liquid-state nuclear magnetic resonance (NMR) spectroscopy.[3] NMR is still at the forefront in terms of the number of qubits (a "quantum bit" consisting of two states $|0\rangle$ and $|1\rangle$) that have been harnessed for running quantum computing algorithms, setting the current world record at seven. Unfortunately, this number is unlikely to grow beyond ten or so due to the noise which accumulates in the NMR signal as the size of the molecule increases. The qubits in NMR are the nuclear spins of atoms, and the number of qubits is equal to the number of atoms. A promising new approach for realizing a quantum computer is based on using the vibrational states of molecules to represent qubits.[4] In this approach, the number of qubits is proportional to the number of vibrational degrees of freedom which is given by $3N-6$ for a N-atom molecule. The vibrational state approach has several advantages over NMR: (i) More qubits can be realized using a N-atom molecule, (ii) the vibrational states of molecules are stable (over the time scales of interest) and no additional "refocusing" pulses are needed, (iii) the number of qubits is not limited to ten, and (iv) by using more vibrational states, it may be possible to represent quantum information units having more than two states (i.e., $|0\rangle$, $|1\rangle$, $|2\rangle$, $|3\rangle$,...). In the vibrational state approach, quantum logic operations are performed by applying femtosecond infrared laser pulses optimized to induce the desired vibrational transitions. This approach potentially meets all five of DiVincenzo's principal criteria,[5] while additionally offering an advantage of high-speed operation. It may be the technology that will realize the dream of quantum computing one day.

Several pioneering papers on this subject have been published in recent years by Vivie-Riedle and co-workers.[4,6,7] They studied theoretically a two-qubit system implemented as two normal vibrational modes of the acetylene molecule (C_2H_2). Two vibrational eigenstates in each normal mode were chosen to represent the $|0\rangle$ and $|1\rangle$ states of each qubit. A number of important aspects were clarified for C_2H_2, including the first prediction of optimally shaped pulses for several key gate operations, creation of entangled qubit states, investigation of decoherence sources, and proposals of pathways for experimental realization. The particular choice of acetylene (C_2H_2) was made mostly due to historic reasons: the authors performed the coherent control studies of C_2H_2 in their earlier work[8] and had the potential energy surface and the dipole-moment function for C_2H_2 available. It remains unclear how good or bad the gas phase acetylene molecule is in general for the purpose of quantum computing. There may be better choices. A question "*How to choose the best possible molecular medium for practical realization*

of a quantum computer?'' has never yet been addressed in the literature but will become important one day for those who plan to set up the first experiment.

It is very likely that the first experimental proof-of-principle study will start with simple one-qubit operations. Therefore, in this paper we focus on a one vibrational degree of freedom example (i.e., a one-qubit system). Instead of attacking any particular molecule or any particular normal mode in a chosen real world molecule, we consider a model system where we are free to vary, in physically reasonable ranges, several parameters of the molecule and the pulse. In this way, we are able to model many different systems and determine general trends that affect, for example, the maximum achievable accuracy of gate operations. The accuracy (or fidelity) of gate operations is a very important issue in the context of quantum computing and it was relatively low ($\sim$70%) in the first paper on C_2H_2.[4] That may be the reason why many scientists were quite skeptical about molecular eigenstates as a valid approach to quantum computing. Later, a new method for optimizing the pulse shape was developed with special emphasis on application to quantum computing[6,9] and a dramatic improvement in gate fidelity ($\sim$90%) was achieved. However, this still may not be enough to safely perform tens of gates, one after another, as a part of a quantum computing algorithm.[10] (This situation is very different from all other fields of quantum dynamics where the principle of optimal control has been employed. In almost any other application based on pulse shaping, a slight increase in the ratio of the desired to undesired events is considered a big success.) Therefore, many scientists who discuss the possibility of a practical realization keep asking the question: ''*Is it possible, in principle and in practice, to improve the gate fidelity, by how much and how*?'' In a recent paper published by Rabitz and co-workers, a new way of looking at this problem on very general grounds was presented.[11] Their work shows that in principle all solutions of the optimal control problem are perfect, but access to some of them can be limited by various control constraints. This important finding brings more optimism into the overall field of optimal control and, in particular, makes the molecular vibrations approach to quantum computing look very promising. In this paper, we use a complementary approach and perform several numerical ''experiments'' to determine quantitatively to what extent the experimentally relevant constraints limit the achievable accuracy of quantum gates and what can be learned by relaxing those constraints. Results of this study should be especially helpful in designing an experimental scheme for the practical demonstration of quantum information processing using the vibrational eigenstates of molecules.

This paper is organized as follows: In Sec. II optimal control theory is reviewed as applied to the quantum computing problem. In Sec. III we describe our model system, calculate the optimal pulses for the gates NOT and Hadamard rotation, and discuss advantages of the numerical method used here for the time propagation. In Sec. IV we demonstrate the effect of the anharmonicity parameter and several constraints on the achievable accuracy of gates. Some conclusions are given in Sec. V.

II. OPTIMAL CONTROL THEORY

We follow the methodology of Vivie-Riedle[6,7] which, in turn, is based on the iterative method of Rabitz.[12] Although this technique has already been briefly described and employed in the literature, the final equations [Eqs. (6)–(8) below] were not published. For the purpose of completeness and also in order to introduce the notation, we briefly present them here.

The traditional purpose of optimal control theory is to calculate the shape of the laser pulse $\varepsilon(t)$ which induces the maximum transfer of probability from the given initial vibrational state ϕ_i to a chosen final state ϕ_f within the time interval T, called the target time. This is achieved by maximizing the objective functional, defined as[12]

$$J_{fi} \equiv |\langle \psi_i(T)|\phi_f\rangle|^2 - \int_0^T \alpha |\varepsilon(t)|^2 dt$$

$$-2\,\mathrm{Re}\left\{ \langle \psi_i(T)|\phi_f\rangle \int_0^T \langle \psi_f(t)| \frac{i}{\hbar}[H_0 - \mu\varepsilon(t)] \right.$$

$$\left. + \frac{\partial}{\partial t}|\psi_i(t)\rangle dt \right\}. \tag{1}$$

Here $\psi_i(t)$ is the time-dependent wave function of the system driven by the laser pulse $\varepsilon(t)$ from its initial state $\psi_i(t=0)=\phi_i$ to the target state $\psi_i(t=T)=\phi_f$. The first term in the functional (1) serves to maximize the population transfer and the second term is needed to minimize the energy of the laser field. The last term is used to satisfy the time-dependent Schrödinger equation for molecule-light interaction; there $H_0(r) = -1/2m\,\Delta_r + V(r)$ is the time-independent molecular Hamiltonian and $\mu(r)$ is the molecular dipole-moment function. The $\langle \psi_f(t)|$ plays the role of a Lagrange multiplier, while the multiplicative term $\langle \psi_i(T)|\phi_f\rangle$ (Ref. 12) is important to decouple the boundary conditions for $\psi_i(t)$ and $\psi_f(t)$. The function α is a penalty function, used also for the smooth switching-on and switching-off of the pulse[13]

$$\alpha = \alpha(t) = \frac{\alpha_0}{s(t)}, \tag{2}$$

where α_0 is a constant penalty factor, $s(t)$ plays a role of a pulse envelope and can be any smooth function. Everywhere through this paper, except Sec. IV C, we use a simple previously proposed function[13]

$$\alpha_0 = 1, \quad s(t) = \sin^2\left(\pi\frac{t}{T}\right). \tag{3}$$

Such a formulation of the optimal control problem can be applied to a case when we want to optimize one chosen transition, for example, to transfer the population from one vibrational state to another: $|v=0\rangle \rightarrow |v=1\rangle$. Here $\phi_i=|0\rangle$ and $\phi_f=|1\rangle$. There are several references in the literature where such pulses have been calculated for model and real problems.[8,13,14]

Because we are interested in quantum computing, we have to deal with the gate transformations of the vibrational qubit and such a problem is slightly more complex. For ex-

ample, for the gate NOT we have to find a pulse, which induces not just one, but two transitions between the qubit states simultaneously:

$$NOT|0\rangle \rightarrow |1\rangle, \tag{4a}$$

$$NOT|1\rangle \rightarrow |0\rangle. \tag{4b}$$

This means, if the system was initially in the vibrational state $|0\rangle$ it should be driven into the state $|1\rangle$, but if it was initially in the state $|1\rangle$ it should be driven into the state $|0\rangle$. One universal gate pulse should be able to perform each of these two transformations; which one is actually performed depends only on the initial state of the qubit. Therefore, in searching for a gate pulse, one has to generalize the objective functional in order to perform the optimization of the population transfer for two transitions of interest simultaneously. One straightforward way of doing this was recently proposed and consists in maximizing the functional where the sum over the two transitions of interest is introduced:[6]

$$K_{fi} \equiv \sum_{k=1,2} (|\langle \psi_i^k(T)|\phi_f^k\rangle|^2) - \int_0^T \alpha|\varepsilon(t)|^2 dt$$

$$- \sum_{k=1,2} 2\,\mathrm{Re}\left\{ \langle \psi_i^k(T)|\phi_f^k\rangle \int_0^T \langle \psi_f^k(t)| \frac{i}{\hbar}[H_0 \right.$$

$$\left. - \mu\varepsilon(t)] + \frac{\partial}{\partial t}|\psi_i^k(t)\rangle dt \right\}. \tag{5}$$

The index k labels the two transitions of interest, so that for the gate NOT, we set, $\phi_i^1=|0\rangle$, $\phi_f^1=|1\rangle$, and $\phi_i^2=|1\rangle$, $\phi_f^2=|0\rangle$. The $\psi_i^k(t)$, $k=\{1,2\}$, are the laser-driven time-dependent wave functions for each case, and $\varepsilon(t)$ is the universal gate field.

The final goal, derivation of the equations for calculation of the optimal pulse $\varepsilon(t)$, is accomplished by maximizing the functional with respect to variations in five functions: $\psi_f^k(t)$, $\psi_i^k(t)$, $k=\{1,2\}$, and $\varepsilon(t)$. This procedure is very similar to the maximization of the functional (1) described in detail in the literature.[13] Applying variations of $\psi_f^1(t)$ and $\psi_f^2(t)$ to the functional (5) we obtain in each case

$$i\hbar \frac{\partial}{\partial t}\psi_i^k(t) = [H_0 - \mu\varepsilon(t)]\psi_i^k(t),$$

$$\psi_i^k(0) = \phi_i^k, \quad k=\{1,2\}. \tag{6}$$

These are two time-dependent Schrödinger equations for the molecule-light interaction to be propagated forward in time, each one with its own initial condition ϕ_i^k. Furthermore, variations of $\psi_i^1(t)$ and $\psi_i^2(t)$ in the functional (5) give

$$i\hbar \frac{\partial}{\partial t}\psi_f^k(t) = [H_0 - \mu\varepsilon(t)]\psi_f^k(t),$$

$$\psi_f^k(T) = \phi_f^k, \quad k=\{1,2\}. \tag{7}$$

These are two time-dependent Schrödinger equations for the molecule-light interaction to be propagated backward in time, each one with its own target state ϕ_f^k as a boundary condition. Finally, the variation in $\varepsilon(t)$ gives

$$\varepsilon(t) = -\frac{s(t)}{\hbar\alpha_0}\,\mathrm{Im}\sum_{k=1,2} \langle \psi_i^k(t)|\psi_f^k(t)\rangle\langle \psi_f^k(t)|\mu|\psi_i^k(t)\rangle, \tag{8}$$

where the sum is over the two transitions of interest. We note that the four Schrödinger equations (6) and (7) are coupled only through the field equation (8).

The system of coupled equations (6)–(8) is solved numerically using an iterative method.[12] Iterations start with some reasonable initial guess for $\varepsilon(t)$ and, at first, only the Eqs. (7) are propagated backward in time to determine an initial approximation to $\psi_f^k(t)$, $k=\{1,2\}$. Then the coupled equations (6) and (8) are propagated forward in time using $\psi_f^k(t)$ from the previous step when computing the field according to Eq. (8). This gives the initial approximation to $\psi_i^k(t)$, $k=\{1,2\}$, which is now used in the field equation (8) to propagate backward in time the coupled equations (7) and (8). The iterative procedure continues in this way, and $\varepsilon(t)$ is improved in each iteration, until the desired convergence is achieved.

A slightly more general approach, which gives essentially the same equations, was recently proposed by Palao and Kosloff.[9] The result (6)–(8) is naturally extended onto a system having more then one qubit.[6] Thus, a gate in a two-qubit system (controlled not CNOT for example) involves four transitions

$$CNOT|00\rangle \rightarrow |00\rangle,$$

$$CNOT|01\rangle \rightarrow |01\rangle,$$

$$CNOT|10\rangle \rightarrow |11\rangle,$$

$$CNOT|11\rangle \rightarrow |10\rangle,$$

and the sum in the functional (5) is over the four transitions of interest, so that there are four two-dimensional Schrödinger equations to propagate forward and four backward in time and there are four terms in the sum of Eq. (8) and so on.

III. NOT AND HADAMARD GATES

Here we numerically solve Eqs. (6)–(8) to calculate the optimal pulses for the gates NOT and Hadamard rotation in a one-qubit system implemented as the ground vibrational state, $|0\rangle$, and the first excited vibrational state $|1\rangle$ of the OH diatomic molecule. This diatomic molecule has been used as a benchmark system for many coherent control studies focused on performing one state-to-state transition at a time.[12,13,15] A coherent control study of quantum gates in the OH diatomic, to the best of our knowledge, has never been presented before.

The treatment of the OH diatomic is simplified by the possibility to accurately approximate its potential curve with an analytic Morse oscillator function of the following form:

$$V(r) = -D + D[e^{-a(r-r_e)} - 1]^2. \tag{9}$$

Eigenvalues of the Morse oscillator are given by[15,16]

$$E_v = -D + \omega\left(v + \frac{1}{2}\right) - \Delta\left(v + \frac{1}{2}\right)^2, \tag{10}$$

where ω is harmonic frequency and Δ is the anharmonicity parameter defined as

$$\omega \equiv a\sqrt{\frac{2D}{m}}, \quad \Delta \equiv \frac{a^2}{2m}. \tag{11}$$

All of the necessary Morse eigenfunctions $\varphi_v(r)$ can be easily computed using a recursive scheme.[17] The dipole-moment function is also taken to be the analytic form:

$$\mu(r) = \mu_0 r e^{-r/r_0}. \tag{12}$$

In this section we use a standard set of Morse parameters for the OH diatomic, namely, $D=0.1994$, $r_e=1.821$, $a=1.189$, $\mu_0=3.088$, $r_0=0.6$ (all numbers are given in atomic units), and the target time $T=750$ fs. The initial guess pulse was taken as

$$\varepsilon(t) = \varepsilon_0 \sin(\omega_{|0\rangle\leftrightarrow|1\rangle}t)s(t), \tag{13}$$

where $\varepsilon_0=0.005$ is a pulse amplitude (in atomic units) and $\omega_{|0\rangle\leftrightarrow|1\rangle}=E_{|1\rangle}-E_{|0\rangle}$ is the frequency for the $|0\rangle\rightarrow|1\rangle$ and $|1\rangle\rightarrow|0\rangle$ transitions, and $s(t)$ is the shape function from Eq. (3).

During the iterative procedure of solving Eqs. (6)–(8) we can analyze the laser-driven wave functions ψ^k after each propagation step by simply projecting them onto the corresponding wave functions ϕ^k. Namely, the backward propagated wave functions ψ_f^k are projected onto the corresponding initial qubit states ϕ_i^k, while the forward propagated wave functions ψ_i^k are finally projected onto the corresponding final qubit states ϕ_f^k:

$$P_f^k = |\langle\phi_i^k|\psi_f^k(t=0)\rangle|^2, \quad k=\{1,2\}, \tag{14}$$

$$P_i^k = |\langle\phi_f^k|\psi_i^k(t=T)\rangle|^2, \quad k=\{1,2\}. \tag{15}$$

The four numbers P_i^k, P_f^k, $k=\{1,2\}$ reflect the accuracy or fidelity of the gate pulse. They can also be used to determine the convergence of the iterative procedure. In Fig. 1 we plot P_i^1 and P_f^1 for 3001 propagation steps (i.e., for 1501 backward-forward propagation iteration loops) during the optimization of a pulse for the NOT gate in the OH diatomic (note: in this case the P_i^2 and P_f^2 are hardly distinguishable from the P_i^1 and P_f^1 at the scale of Fig. 1 and are not plotted). The backward propagation steps are labeled by even numbers starting from zero and are shown as circles and the forward propagation steps are labeled by odd numbers starting from one and are shown as diamonds. All four curves are smooth and convergence is monotonic. The four values of $P_{i,f}^{1,2}$ are converged within 10^{-4} in about 350 propagation steps, within 10^{-5} in about 500 steps, and within 10^{-6} in about 800 steps. The converged value of $P_{i,f}^{1,2}$, which can be regarded as the fidelity of the pulse, is $P_{i,f}^{1,2}=0.994\,813$ (see the insert in Fig. 1). All 3001 propagation steps are performed in order to check that the solution is stable and nothing unexpected happens if iterations continue after the desired convergence is already achieved.

Figure 2(a) shows the optimized laser pulse $\varepsilon(t)$ for the gate NOT in the OH diatomic obtained after 3001 propagation steps. Figures 2(b) and 2(c) show how the population of the vibrational qubit states $|0\rangle$ and $|1\rangle$ changes as a function of time for transitions (4a) and (4b), respectively, when the
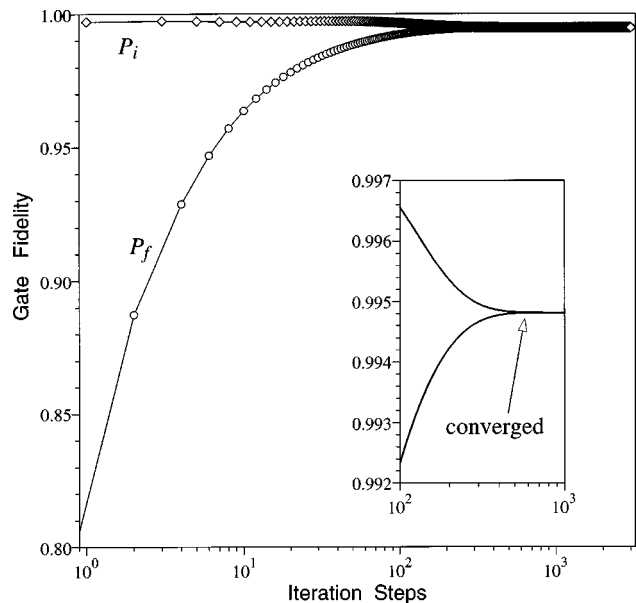

FIG. 1. Illustration of the convergence studies for the gate NOT in the OH diatomic. The fidelity functions P_i and P_f are defined in Eqs. (13) and (14). The insert is used to show the same two curves in detail in the asymptotic region. See text for further details.

pulse in Fig. 2(a) is applied to OH. The pulse shape is very symmetric and quite simple because there is only one characteristic frequency in the process, $\omega_{|0\rangle\leftrightarrow|1\rangle}$. This was confirmed by the Fourier analysis of the gate pulse given in Fig. 2(a). The time profiles of the population transfer between the qubit states presented in Figs. 2(b) and 2(c) are also symmetric and simple. Insert in the Fig. 2(b) exhibits the fine structure of the profiles: in all cases there are small regular oscillations superimposed with the monotonic decrease/growth of the probability. Similar behavior has already been described in the literature (see Fig. 13 in Ref. 18). These oscillations are a reflection of the pulse action. Their frequency is twice the frequency of the pulse, $2\times\omega_{|0\rangle\leftrightarrow|1\rangle}$. (The double frequency can also be found in the literature in the oscillations of the second order momenta $\langle q^2\rangle$ and $\langle p^2\rangle$ (Ref. 19) and width[20] of a semiclassical wave packet, for example.) Finally, Fig. 2(d) shows the time evolution of population in several upper vibrational states of OH diatomic during the NOT pulse for the case of transition (4a) [the case of transition (4b) is very similar]. These vibrational states, $v=|2\rangle$, $|3\rangle$, $|4\rangle$, $|5\rangle$ etc., are the states interfering with the states of the vibrational qubit $|0\rangle$ and $|1\rangle$. Note the logarithmic scale of the probability. At this scale the curves in Fig. 2(d) exhibit some visible deviation from a perfectly symmetric shape and show some negligible ($\sim 10^{-6}$) residual population in the state $|2\rangle$.

The Hadamard rotation (HAD) is another very important gate in quantum computing:

$$\text{HAD}|0\rangle \rightarrow \frac{1}{\sqrt{2}}|0\rangle + \frac{1}{\sqrt{2}}|1\rangle, \tag{16a}$$

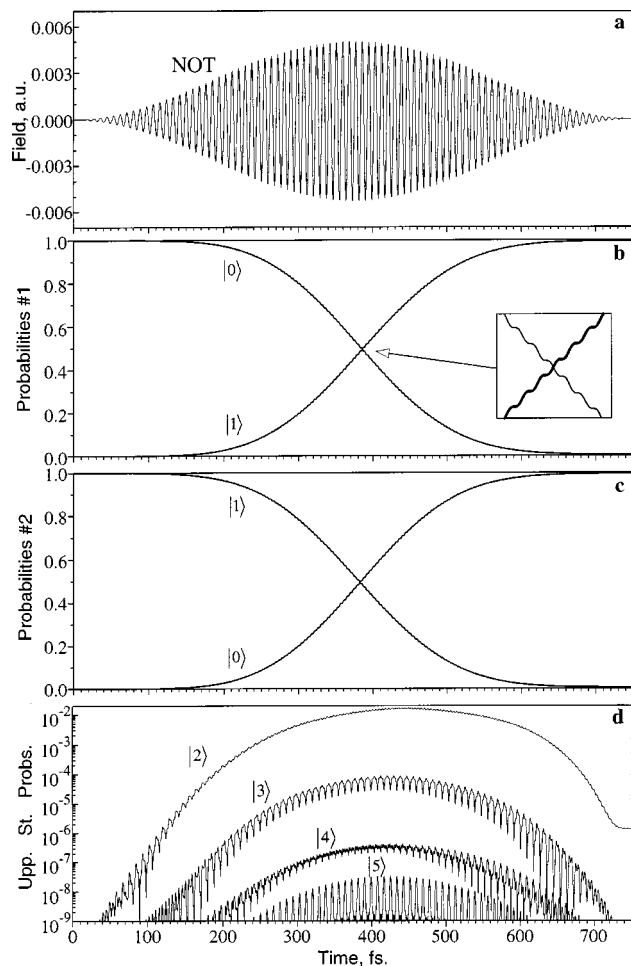$$\text{HAD}|1\rangle \rightarrow \frac{1}{\sqrt{2}}|0\rangle - \frac{1}{\sqrt{2}}|1\rangle. \tag{16b}$$

FIG. 2. The gate NOT in the OH diatomic. The qubit states are the ground and the first excited states $|0\rangle$ and $|1\rangle$. The target time is 750 fs. (a) Optimally shaped pulse; (b) Switching of population between the qubit states during the NOT$|0\rangle\rightarrow|1\rangle$ transformation; (c) Switching of population between the qubit states during the NOT$|1\rangle\rightarrow|0\rangle$ transformation; (d) Populations of all upper vibrational states during the gate remains small and their residual populations are negligible.

FIG. 3. Hadamard rotation in the OH diatomic. The qubit states are the ground and the first excited states $|0\rangle$ and $|1\rangle$. The target time is 750 fs. (a) Optimally shaped pulse; (b) Creation of linear superposition of the qubit states as required by HAD$|0\rangle\rightarrow 1/\sqrt{2}\,|0\rangle + 1/\sqrt{2}\,|1\rangle$; (c) Creation of linear superposition of the qubit states as required by HAD$|1\rangle\rightarrow 1/\sqrt{2}\,|0\rangle - 1/\sqrt{2}\,|1\rangle$; (d) Populations of all upper vibrational states during the gate remains small and their residual populations are negligible.

Figures 3(a)–3(d) illustrate our results for this gate in the OH diatomic [compare to Figs. 2(a)–2(d) for the gate NOT]. Although the general shape of the Hadamard pulse is very similar to the shape of the NOT pulse, the field amplitude is about twice smaller in the case of the Hadamard gate [note different scales in Figs. 2(a) and 3(a)]. This is because in the case of the Hadamard gate we need to transfer only $\frac{1}{2}$ of the population between the qubit states $|0\rangle$ and $|1\rangle$, which is clearly reflected in the Figs. 3(b) and 3(c). Therefore, the Hadamard gate is easier to implement in a sense of population transfer and energy required. For this reason the fidelity of the converged Hadamard pulse that we have obtained is considerably larger, $P_{i,f}^{1,2}=0.998\,759$. We have also observed that the population of the upper vibrational states is smaller in the case of the Hadamard gate [note different scales in Figs. 2(d) and 3(d) and the fact that the vibrational state $v=|5\rangle$ is not seen above 10^{-9} at all].

We have intentionally postponed the discussion of the numerical scheme for the time propagation of the Schrödinger equations (6) and (7) until now. Figures 2(d) and 3(d) clearly show that only a few vibrational states of the OH
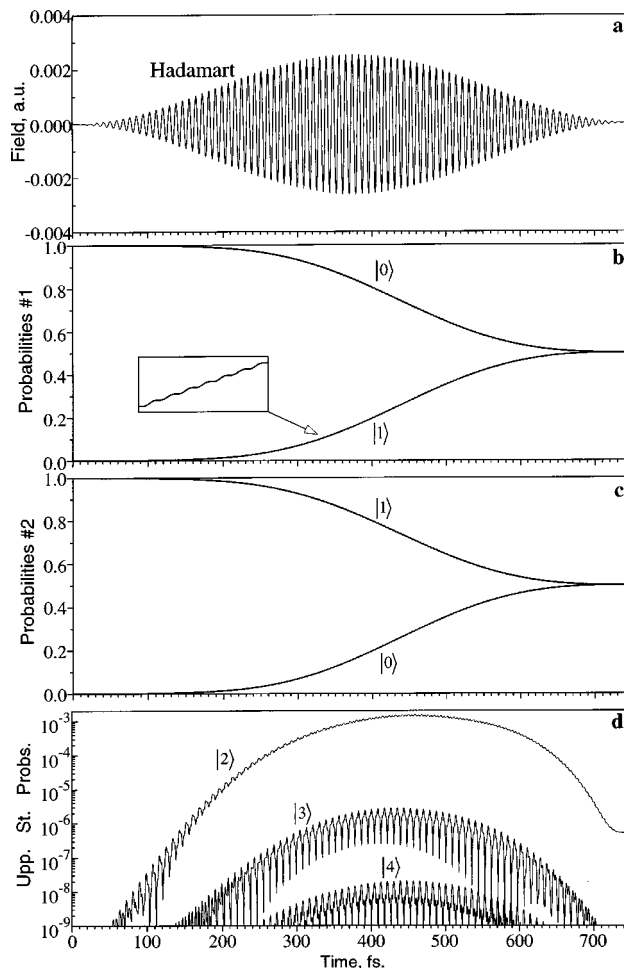
diatomic acquire a significant population during the gate pulse. These are, of course, the qubit states $v=|0\rangle$ and $|1\rangle$ and, if we set up the probability cutoff value at 10^{-6}, the vibrational states $|2\rangle$ and $|3\rangle$. If the probability cutoff is set at 10^{-9} the vibrational states $|4\rangle$ and $|5\rangle$ should also be included. In any case, we are dealing here with a very simple wave packet $\psi(t)$ consisting almost entirely of two vibrational eigenstates, with a small participation of the third and only a tiny contribution of upper eigenstates. In such a situation, the most efficient scheme for time propagation is the expansion of the wave packet $\psi(t)$ in the basis set of vibrational eigenstates (Morse oscillator eigenfunctions $\varphi_v(r)$ in our case) with time dependent complex coefficients and propagating the system of coupled equations for these coefficients forward and backward in time as required by Eqs. (6) and (7). Convergence studies have shown that using just three lower eigenstates as a basis set produces very reasonable results and using more than six eigenstates in a basis set is unnecessary. Therefore, the size of the system of coupled equations is quite small and the time propagation is very fast and accurate using, for example, the fourth-order Runge-

Kutta method.[21] We employed the interaction representation to analytically factor out all oscillatory phases; this way we are able to use a larger time step ($\Delta t = 10$ a.u.). The dipole-moment matrix elements $\mu_{ij} = \langle \varphi_j(r) | \mu(r) | \varphi_i(r) \rangle$ are computed only once and are stored in memory. Therefore, we suggest that basis set expansion is the method of choice for the numerical modeling of optimal pulses for quantum computer gates—a problem where very few vibrational eigenstates are effectively involved in the process.

IV. EFFECT OF VARIOUS FACTORS ON ACCURACY OF GATES

A. Anharmonicity parameter

The vibrational spectrum of the Morse oscillator is determined by two factors: the harmonic frequency ω and anharmonicity parameter Δ [see Eq. (10)]. In the limiting case $\Delta \to 0$, it becomes the spectrum of the Harmonic oscillator where all the levels are equidistant and simultaneously accessible by the single frequency ω through the step-ladder process. It is intuitively clear that such a system can not be controlled since there is no way to differentiate between the various interfering state-to-state transitions. We have confirmed this in numerical tests; for rigorous theoretical proof see Ref. 22 and references therein. In another limiting case, when $\Delta \to \infty$ and transitions to upper vibrational states are impossible due to practically limited spectral bandwidth, it is also intuitively clear that the oscillator becomes equivalent to an isolated two-level system and can be perfectly controlled. Real life molecules are somewhere between these two limiting cases, and it is interesting to determine quantitatively how the magnitude of anharmonicity parameter Δ affects the accuracy of quantum gates.

In the case of the OH diatomic, $\omega = 3964$ cm^{-1} and $\Delta = 89.75$ cm$^{-1} \approx 90$ cm^{-1}. Here we will explore the physically relevant wide range of the anharmonicity parameter: $10 \leqslant \Delta \leqslant 110$ cm^{-1}. This is achieved by constructing several different model Morse potentials, all with the same values of m, ω, and r_e as in real OH, but with different values of anharmonicity Δ. The values of parameters a and D should also change according to,

$$a = \sqrt{2m\Delta}, \tag{17}$$

$$D = \frac{\omega^2}{4\Delta}. \tag{18}$$

In this way, we can consider the harmonic frequency as fixed, $\omega = $ const, while the anharmonicity parameter Δ can be varied within the desired limits. The two parameters for the dipole-moment function μ_0 and r_0 are also kept constant and equal to those in the real OH. Figure 4 shows the 14 different model Morse oscillator functions constructed in this way using the values of $\Delta = 10$, 15, 20, 25, 30, 35, 40, 50, 60, 70, 80, $\sim$90, 100, 110 cm^{-1}. The case of real OH is included as $\Delta \sim 90$ cm^{-1} and is shown in bold in Fig. 4. The dissociation energy for different curves in Fig. 4 changes according to Eq. (17). The total number of bound vibrational states also changes as $N = (\omega/2\Delta) - 1/2$ (Ref. 16) but even for the upper, most anharmonic, and the most shallow Morse oscillator
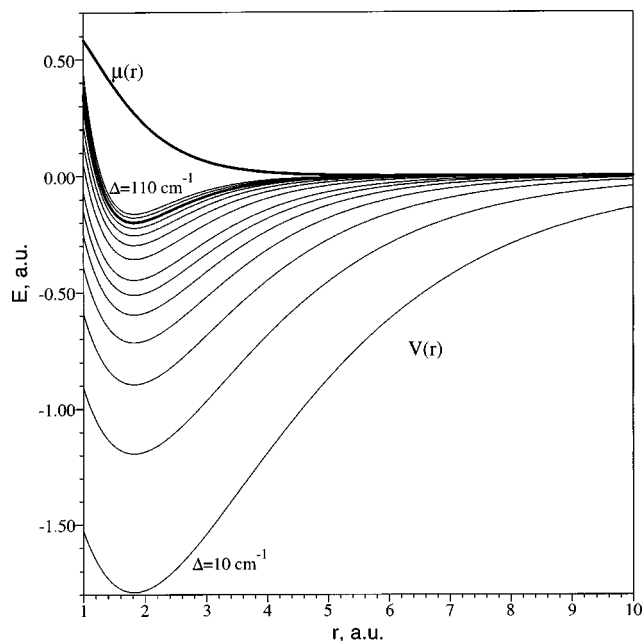

FIG. 4. Morse oscillator functions for the 14 values of anharmonisity parameter within $10 \leqslant \Delta \leqslant 110$ cm^{-1} region considered in this study. See text for further details. The Morse potential and the dipole-moment function for true OH diatomic ($\Delta \approx 90$ cm^{-1}) are shown in bold.

with $\Delta = 110$ cm^{-1}, there are 18 bound states, which is large enough for implementing a qubit and solving the optimal control problem.

We have solved the optimal control problem (6)–(8) for both Hadamard and NOT gates for all the 14 values of Δ using the target time $T = 750$ fs; the results are summarized in Fig. 5. It is clearly seen that the fidelity of the Hadamard gate is always much better than the fidelity of the NOT gate and this is consistent with the discussion in the preceding
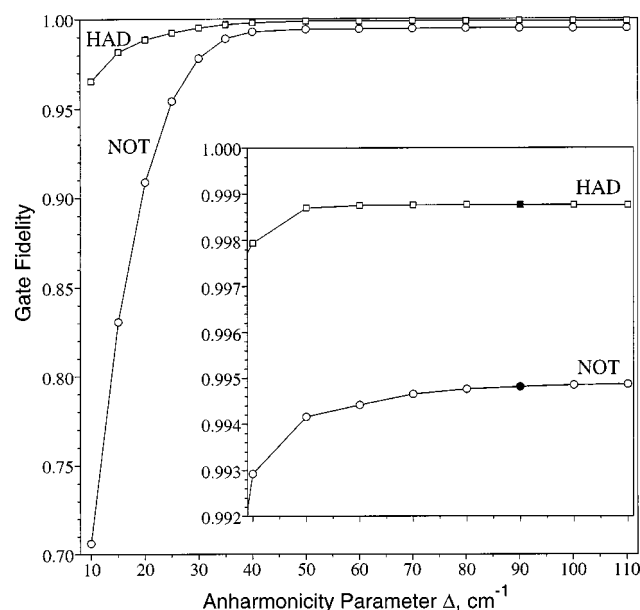

FIG. 5. Fidelities of the gates NOT and Hadamard rotation as a function of anharmonicity parameter of the model system. The insert is used to show the same two curves in detail in the high fidelity plato region. Filled symbols describe the case of true OH diatomic.
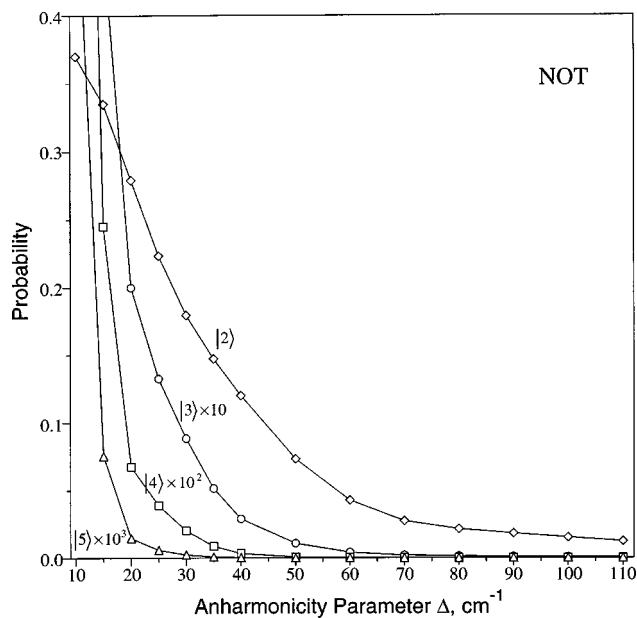
FIG. 6. Populations of upper vibrational states during the gate NOT as a function of anharmonicity parameter of the model system. Note the different scale factors used for different states.

section. As expected, the highest fidelity in each case is achieved with the highest value of $\Delta = 110$ cm^{-1}. It is $P_{i,f}^{1,2}$ $= 0.994\,867$ for the gate NOT and $P_{i,f}^{1,2} = 0.998\,762$ for the Hadamard transform. One important finding is the presence of a high fidelity plateau in the region $50 \leqslant \Delta \leqslant 110$ cm^{-1}. The results for the real OH molecule, discussed in detail in the preceding section ($\Delta \approx 90$ cm^{-1}), are shown as filled symbols in the insert in Fig. 4 and fall onto that plateau. Another important observation from Fig. 5 is a rapid drop of the fidelity of both gates as the value of anharmonicity parameter decreases below the $\Delta = 40$ cm^{-1}.

To understand this behavior we have monitored the populations of upper vibrational states during the gate pulse for all studied values of Δ and have determined the maximum population observed in each state. These data for the states $|2\rangle$, $|3\rangle$, $|4\rangle$, and $|5\rangle$ are presented in Fig. 6 for the gate NOT (note: the scale factors are different for different states). This figure illustrates that for the values of anharmonicity parameter in the plateau region, $50 \leqslant \Delta \leqslant 110$ cm^{-1}, the population of the upper vibrational states during the process remains relatively small, but it increases significantly as Δ decreases below $\Delta = 40$ cm^{-1}. This behavior correlates with the behavior of the gate fidelity shown in Fig. 5 and we believe that the explanation of the observed dependencies is as follows. When the Δ is large the molecule is closer to the hypothetic two-level system. For example, for $\Delta = 110$ cm^{-1} the maximum population observed in the state $|2\rangle$ during the gate pulse is only ~ 0.01 and the populations of all higher states are negligible. Such a system is easy to control. However, when Δ is small, the probability flows easily in at least several upper states as demonstrated in Fig. 6 and the system is closer to another limit, the harmonic oscillator, and is hard to control. As a result, the fidelity of the gates drops.

We have also examined the residual populations of upper

vibrational states at the end of the pulse $t = T$, for all values of Δ. It appears that in all cases the residual population of upper states is much smaller than the maximum population of these states found during the gate pulse and shown in Fig. 5. The optimized pulse is always able to return most of the population from the interfering upper states back into the qubit states as it is shown in Figs. 2(d) and 3(d). For practical values of the anharmonicity parameter in the high fidelity plateau region, $50 \leqslant \Delta \leqslant 110$ cm^{-1}, the residual population of upper states is always tiny ($\sim 10^{-6}$) and it seems more appropriate to disregard it and to correlate the maximum population observed in the upper states during the pulse (Fig. 5) with the fidelity of gates (Fig. 4). We just want to mention that in the low fidelity region, $\Delta \leqslant 40$ cm^{-1}, there is some finite residual population of the upper states. There one may want to try to correlate the residual population with the fidelity of gates.

B. Target time

In this section we study the effect of the target time T on the fidelity of the gates. We have chosen three values of the anharmonicity parameter $\Delta = 30$, 60 cm^{-1}, and $\Delta \approx 90$ cm^{-1} (true OH) to represent the high fidelity plateau and the transition region. The target time is varied in the limits $500 \leqslant T \leqslant 1000$ fs, so that the results of the preceding sections obtained at $T = 750$ fs are right in the middle of the time interval studied here. We have solved the optimal control problem (6)–(8) for 11 different values of target time T and results for the gate NOT are presented in Fig. 7 (the results for Hadamard gate are qualitatively similar). In all three cases, the curves are smooth and the fidelity achieved by the longer pulses is higher. The effect is more pronounced for the case of $\Delta = 30$ cm^{-1}, where increasing the target time from 500 to 1000 fs allows for the recovery of more than 10% of the gate fidelity [see Fig. 7(b)]. This makes the case of $\Delta = 30$ cm^{-1} almost as accurate as the $\Delta = 60$ cm^{-1} and $\Delta \approx 90$ cm^{-1} cases. The fidelities achieved with the highest value of $T = 1000$ fs are $P_{i,f}^{1,2} = 0.995\,848$, $P_{i,f}^{1,2} = 0.997\,017$, and $P_{i,f}^{1,2} = 0.997\,094$, respectively.

To understand this effect we have inspected the optimized pulses for different values of the target time and have found that the amplitude of the laser field smoothly decreases as the target time increases. For example, in the spectacular case of $\Delta = 30$ cm^{-1} the maximum value of the electric field (achieved in the middle of the optimized pulse) is $\varepsilon_{max} = 0.008\,61$ a.u. for $T = 500$ fs and is only $\varepsilon_{max} = 0.004\,34$ a.u. for $T = 1000$ fs. This result is well understood since a longer action time, assigned to perform the same state-to-state transition in a qubit, allows using the field of smaller amplitude. However, we have also observed very clearly that in those cases when the field is higher (the target time is shorter) the upper interfering states acquire higher populations during the pulse. Thus, the arguments of the preceding section about the effect of involvement of the upper states on accuracy of gates are applicable here as well, though the effect is indirect in the following sense: increasing the pulse target time we decrease the field amplitude and, as a result, decrease the participation of interfering upper
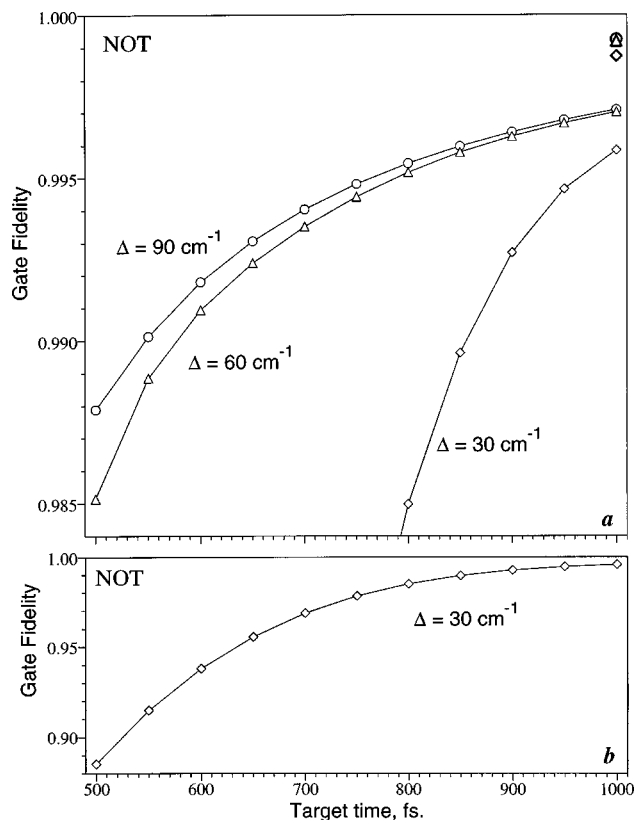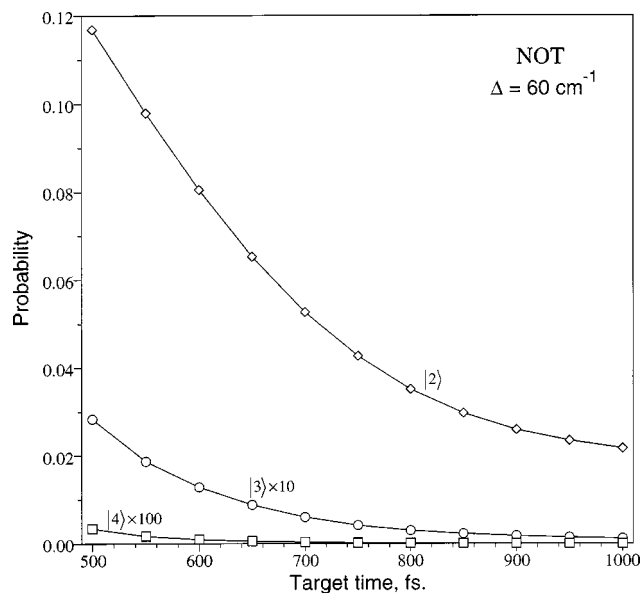
FIG. 8. Populations of upper vibrational states during the gate NOT as a function of pulse's target time for a model system with the medium value of anharmonicity parameter $\Delta = 60$ cm^{-1}.

FIG. 7. Fidelity of the gate NOT as a function of pulse's target time for the three systems with anharmonicity parameters $\Delta = 30$, 60 cm^{-1} and $\Delta \approx 90$ cm^{-1} (true OH diatomic). Three symbols in bold in the upper right corner show the results obtained without any penalty function (Sec. 4 C). Frame (b) is used to show the case $\Delta = 30$ cm^{-1} at the different scale, so that the increase in gate fidelity by more than 10% is clearly seen.

states in the process, which in turn increases the fidelity of qubit transformation.

By analogy with Fig. 6 we have monitored the populations of upper vibrational states during the gate pulse and plotted the maximum values of the probability observed in those states, but now as a function of the target time T of the pulse. We have done this for all 11 values of the target time in the interval $500 \leq T \leq 1000$ fs and the three values of anharmonicity parameter studied in this subsection. In all three cases we have found that the population of the upper vibrational states drops as the target time T increases. The results for the gate NOT in the case of intermediate value of anharmonicity parameter $\Delta = 60$ cm^{-1} are presented in Fig. 8. It is quite interesting that the general behavior of the curves in Fig. 8 is qualitatively similar to that seen in Fig. 6. This is despite the fact that the two absolutely different parameters (anharmonicity in Fig. 6 and the target time in Fig. 8) are plotted along the horizontal axis. Shapes of the curves in Fig. 8 correlate very well with the shape of the fidelity curve in Fig. 7 and we believe this can serve as a proof of the effect discussed in the preceding paragraph.

C. Penalty function

The final constraint we examine is the penalty function $s(t)$. For the cases $\Delta = 30$, 60 cm^{-1}, and $\Delta \approx 90$ cm^{-1} and the target time $T = 1000$ fs we have solved the optimal con-

trol problem (6)–(8) using $s(t) = 1$, i.e., without any penalty function. The shape of the pulse optimized in the absence of $s(t)$ is different from the shape given in Figs. 2(a) and 3(a). Now we are dealing with the pulses that start and stop abruptly, showing almost constant amplitude of the field through the pulse duration (less than 10% deviation, almost rectangular pulses). Such pulses are very difficult to produce experimentally and we consider them here only as a limiting case. The fidelity of the gate NOT achieved in this case for all three values of Δ is very high, around 0.999 (see Fig. 7, bold symbols in the upper right corner).

Not only the general shape of the optimized pulses changes, but also the amplitude of the field changes significantly. Thus, in the case of $\Delta \approx 90$ cm^{-1}, $T = 1000$ fs we observed the maximum field amplitude $\varepsilon_{max} = 0.00382$ a.u. for the case of $s(t)$ as in Eq. (3) and only $\varepsilon_{max} = 0.00206$ a.u. for the case of $s(t) = 1$. This is because when the penalty function is used the field amplitude is constrained to increase and decrease very slowly [as in Figs. 2(a) and 3(a)] and the pulse's "effective" action occurs on the time interval shorter that T. In other words, the pulse duration is truncated by the penalty function and a field amplitude must be larger near the center of the pulse ($t \sim T/2$), compare to the amplitude of the flat rectangular pulse, in order to perform the same qubit transformation. However, as we have already explained in the preceding section, larger field amplitude means higher populations of upper vibrational states and lower fidelity of the pulse. We believe such a scheme explains the observed jump of fidelity for rectangular pulses.

V. CONCLUSIONS

In this paper we have studied several properties of a model quantum computer, which uses vibrational eigenstates to implement quantum information bits and uses optimally shaped pulses to operate quantum logic gates. We have dem-

onstrated that a number of factors can and should be employed in order to achieve the high fidelity of gates in such a quantum computer. One of these factors is the anharmonicity parameter of the molecule itself. Indeed, we have observed the high fidelity plateau in the region $50 \leqslant \Delta \leqslant 110 \text{ cm}^{-1}$. In such anharmonic systems, it is easier to achieve a good control over the vibrational processes because the different state-to-state transitions are easier to resolve and, as we have shown, it is easier to restrict the vibrational population of the molecule to the qubit states $|0\rangle$ and $|1\rangle$. Therefore, we suggest that using molecules with large anharmonicity parameters will help significantly in achieving the necessary high fidelity of gates in the vibrational qubit. The anharmonicity parameter of the OH diatomic is $\Delta \approx 90 \text{ cm}^{-1}$, and falls into that range. Naturally, all bonds that involve hydrogen atom are very anharmonic and are good candidates for implementing a vibrational qubit. For example, the anharmonicity parameter of the CH diatomic is $\Delta \approx 63 \text{ cm}^{-1}$ and is also in that range. Among larger real world molecules many hydrocarbons (benzene, naphthalene, etc.) can be good candidates for practical realization of multiple vibrational qubits. In such molecules, there are always several bright IR-active normal vibrational modes associated with CH stretches and those are very anharmonic. Other good candidates can, probably, be found among the molecules that have very unharmonic triple $C \equiv O$ bonds, such as $Rh(CO)_2(C_5H_7O_2)$ (Ref. 23) or $Cr(CO)_6$.[24]

We have observed that the fidelity of quantum gates drops significantly when the anharmonicity parameter is less than $\Delta = 40 \text{ cm}^{-1}$. However, we have also found that even in such cases the fidelity of gates can be improved significantly by relaxing constraints on the shaped pulse. Thus, longer pulses allow using a field of smaller amplitude and avoid putting too much population into the upper vibrational states ($|2\rangle$, $|3\rangle$, $|4\rangle$,...) interfering with the states of the qubit $|0\rangle$ and $|1\rangle$. This permits to use efficiently the molecules with not enough anharmonicity and obtain a much better fidelity of quantum gates.

The effect of the penalty function used to smoothly switch-on and switch-off the optimal pulse is somewhat similar to reducing the pulse duration and is, therefore, negative in a sense of the gate fidelity. Thus, the $\sin^2$ penalty function (3) rises and decays, perhaps too slowly, reaching the unit value only in the middle of the pulse ($t = T/2$) and leaving a very short time for efficient pulse action. This must be compensated by increasing the field amplitude, which increases the population of upper vibrational states and results in lower fidelity of the gates. Therefore, we suggest exploring other forms of the penalty function in order to meet both conditions simultaneously: the smoothly switching-on and switching-off of the pulse and the relatively long time of

efficient pulse action. This can be easily achieved with penalty functions that are flatter than the $\sin^2$ function in Eq. (3).

Furthermore, we have clearly seen that some quantum gates exhibit naturally better fidelity than the others. In all cases considered here the fidelity of the Hadamard rotation was significantly better than the fidelity of the gate NOT. This is because for the Hadamard rotation we need to transfer only $\frac{1}{2}$ of the population between the qubit states. This is achieved using the field of smaller amplitude and results in better gate fidelity.

Finally, we have demonstrated that a quantum computer based on vibrational eigenstates to implement the quantum information bits and optimally shaped laser pulses to apply the quantum logic gates can be a robust tunable system. Carefully choosing various properties of the molecule and of the pulse allows one to achieve very high fidelity gates.

[1] R. Feynman, Int. J. Theor. Phys. **21**, 467 (1982).
[2] G. Johnson, *A Shortcut Through Time: The Path to the Quantum Computer* (Knopf, New York, 2003).
[3] J. A. Jones and M. Mosca, J. Chem. Phys. **109**, 1648 (1998).
[4] C. M. Tesch, L. Kurtz, and R. de Vivie-Riedle, Chem. Phys. Lett. **343**, 633 (2001).
[5] D. P. DiVincenzo and D. Loss, Superlattices Microstruct. **23**, 419 (1998).
[6] C. M. Tesch and R. de Vivie-Riedle, Phys. Rev. Lett. **89**, 157901 (2002).
[7] U. Troppmann, C. M. Tesch, and R. de Vivie-Riedle, Chem. Phys. Lett. **378**, 273 (2003).
[8] C. M. Tesch, K.-L. Kompa, and R. de Vivie-Riedle, Chem. Phys. **267**, 173 (2001).
[9] J. P. Palao and R. Kosloff, Phys. Rev. Lett. **89**, 188301 (2002).
[10] N. G. Cooper and J. A. Schecker. *Information, Science, and Technology in a Quantum World* (Los Alamos, NM, 2003).
[11] H. A. Rabitz, M. M. Hsieh, and C. M. Rosenthal, Science **303**, 1998 (2004).
[12] W. Zhu, J. Botina, and H. Rabitz, J. Chem. Phys. **108**, 1953 (1998).
[13] K. Sundermann and R. de Vivie-Riedle, J. Chem. Phys. **110**, 1896 (1999).
[14] E. Sundermann, H. Rabitz, and R. de Vivie-Riedle, Phys. Rev. A **62**, 013409 (2000).
[15] G. K. Paramonov, Chem. Phys. **177**, 169 (1993).
[16] M. L. Sage, Chem. Phys. **35**, 375 (1978).
[17] H. Kobeissi, J. Comput. Phys. **61**, 351 (1985).
[18] B. M. Garraway and N. V. Vitanov, Phys. Rev. A **55**, 4418 (1997).
[19] E. Pahl and O. V. Prezhdo, J. Chem. Phys. **116**, 8704 (2002).
[20] D. Kilin and M. Schreiber, J. Lumin. **92**, 13 (2001).
[21] W. H. Press, *Numerical Recipes: The Art of Scientific Computing* (Cambridge University, Cambridge, 1986).
[22] V. Ramakrishna, M. V. Salapaka, M. Dahleh, H. Rabitz, and A. Pierce, Phys. Rev. A **51**, 960 (1995).
[23] O. Golonzka, M. Khalil, N. Demirdoven, and A. Tokmakoff, J. Chem. Phys. **115**, 10814 (2001).
[24] L. Windhorn, T. Witte, J. S. Yeston, D. Proch, M. Motzkus, K. L. Kompa, and W. Fuß, Chem. Phys. Lett. **357**, 85 (2002).